NANO LETTERS

Letter

pubs.acs.org/NanoLett

Individual GaN Nanowires Exhibit Strong Piezoelectricity in 3D

Majid Minary-Jolandan, Rodrigo A. Bernal, Irma Kuljanishvili,[‡] Victor Parpoil, and Horacio D. Espinosa*

Department of Mechanical Engineering, Northwestern University, Evanston, Illinois 60208, United States

ABSTRACT: Semiconductor GaN NWs are promising components in next generation nano- and optoelectronic systems. In addition to their direct band gap, they exhibit piezoelectricity, which renders them particularly attractive in energy harvesting applications for self-powered devices. Nanowires are often considered as one-dimensional nanostructures; however, the electromechanical coupling leads to a third rank tensor that for wurtzite crystals (GaN NWs) possesses three independent coefficients, d_{33}, d_{13}, and d_{15}. Therefore, the full piezoelectric characterization of individual GaN NWs requires application of electric fields in different directions and measurements of associated displacements on the order of several picometers. In this Letter, we present an experimental approach based on scanning probe microscopy to directly quantify the three-dimensional piezoelectric response of individual GaN NWs. Experimental results reveal that GaN NWs exhibit strong piezoelectricity in three dimensions, with up to six times the effect in bulk. Based on finite element modeling, this finding has major implication on the design of energy harvesting systems exhibiting unprecedented levels of power density production. The presented method is applicable to other piezoelectric NW materials as well as wires manufactured along different crystallographic orientations.

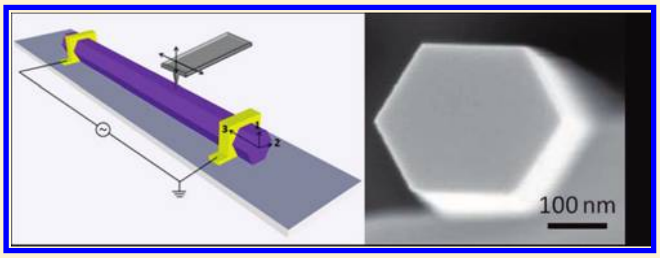

KEYWORDS: *Piezoelectricity, GaN NWs, scanning probe microscopy, piezoresponse force microscopy, nanogenerators*

Nanodevices, such as nanogenerators and optoelectronic devices, rely on semiconductor NWs (NWs) as their building blocks.[1,2] NW-based devices, such as light emitting diodes,[3] lasers,[4] field-effect transistors,[5] and nanogenerators, have already been demonstrated. Understanding the fundamental properties of these building blocks is crucial in designing high-performance and reliable devices. As a result, a great emphasize is placed on probing the electrical, mechanical, and optical properties of semiconductor NWs.[3,5,6] Among semiconductor NWs, piezoelectric NWs, such as GaN and ZnO, are particularly attractive due to their ability to generate electric charges in response to mechanical deformation.[7,8] Due to their excellent mechanical properties arising from a low defect density,[6,9] such NWs can undergo large deformation and hence produce sufficient electrical charges for powering nanodevices, particularly mechanical energies harvested from external sources.[10] Nanowires are often considered as one-dimensional (1D) nanostructures, hence, properties in the axial direction are often the only ones that are investigated. Piezoelectricity, which arises from electromechanical coupling, is a third rank tensor. For wurtzite GaN and ZnO NWs that exhibit hexagonal symmetry, the piezoelectric matrix has three independent coefficients (d_{33}, d_{13}, and d_{15}), and in a complex deformation mode, all three constants contribute to charge (voltage) generation. Piezoelectricity in GaN NWs was demonstrated through voltage generation under applied mechanical deformation. It was shown that the output voltage in GaN is higher than in ZnO NWs.[11−13] Recently, it was also shown that by assembly of GaN NWs, nanogenerators could be fabricated with output voltages up to 1.2 V.[14] However, data on the direct quantification of the piezoelectric constants in *individual* GaN NWs have been elusive. Recently, we have reported strong piezoelectricity in individual GaN NWs, based on quantum mechanical calculations,[8] and experimentally, based on piezoresponse force microscopy (PFM).[15]

The piezoelectric constant of common semiconductor materials is on the order of several pm/V. Hence, the induced displacement under applied electric voltage, on the order of several volts, in these materials would be on the order of several tens of pm. Measurement of such small displacements is nontrivial, particularly for 1D nanostructures with one dimension on the order of 100 nm. To address this challenge, scanning probe microscopy (SPM) methods have been widely used for probing the converse piezoelectric effect at the nanoscale.[16,17] Specifically, PFM has been used to investigate piezoelectricity in ZnO nanobelts,[18] PZT NWs,[19] $BaTiO_3$ NWs,[20,21] sodium niobate NWs,[22] potassium niobate NWs,[23] small perovskite particles,[24] ferroelectric nanoribbons,[25] PZT ribbons,[26] individual collagen fibrils,[27,28] peptide nanotubes,[29] and thin films of III-nitride materials.[30] However, nearly all previous studies provided only one piezoelectric constant, often the one related to the out-of-plane deformation measured from the bending of the cantilever in the PFM setup. However, a full understating of piezoelectricity in these 1D nanostructures and their optimized applications in nanogenerators demands

Received: November 16, 2011
Revised: December 14, 2011
Published: December 22, 2011

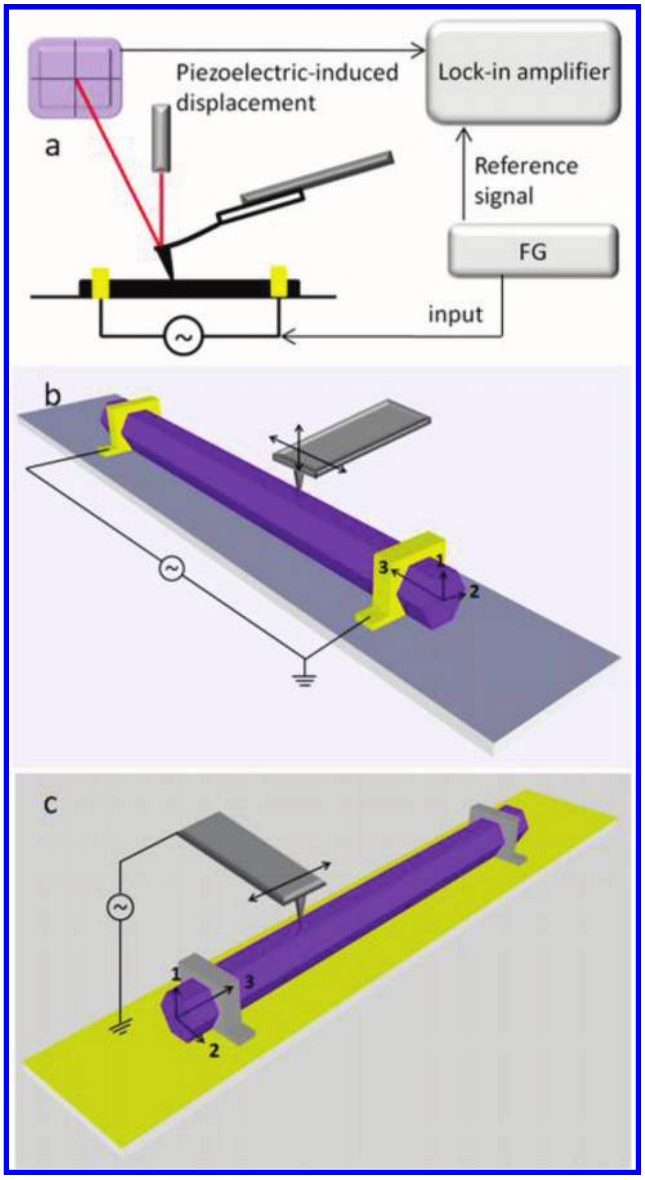

Figure 1. Schematics showing the setup for probing the 3D piezoelectric tensor of a single *c*-axis GaN NW. (a) The experimental setup includes an AFM, a function generator (FG), and a lock-in amplifier. (b) The NW is laying on Si substrate with an insulating SiO_2 layer. The NW is clamped at two ends by metals contacts. An ac voltage is applied between these electrodes, resulting in an axial electric field E_3. The long axis of the NW is placed perpendicular to the AFM cantilever. In this configuration, twist of the cantilever measures the axial displacement, and the bending of the cantilever measures the out-of-plane displacement to obtain d_{33} and d_{13}, respectively. (c) In this configuration the NW is laying on a Si substrate coated with a conductive Au layer. The electric field is applied between the tip of the conductive AFM probe and the grounded substrate, E_1. Torsion of the cantilever measures the induced shear strain allowing identification of d_{15}.

quantifications of all three independent piezoelectric constants. Particularly for *a*-axis $[1\bar{2}10]$ and *m*-axis $[1\bar{1}00]$ GaN NWs, where due to crystallographic orientation, even in pure bending or tension, all three constants contribute to the generated voltage.

In this Letter, we present a method based on SPM to probe the 3D piezoelectric matrix of individual piezoelectric NWs. We leverage the excellent displacement sensitivity of the atomic force microscope (AFM) combined with the dynamic sensitivity of a lock-in amplifier in order to measure small electric field-induced displacements, Figure 1a. Alternating current (ac) voltage is used since measurement of displacement on the order of several pm (several percent of the lattice constant) is more accurate using a lock-in amplifier. Alternating current voltage induces ac oscillations in a piezoelectric material due to changes in lattice configuration. In order to probe piezoelectricity in 3D, we used the torsional twist and flexural bending of an AFM cantilever to measure the harmonic in-plane and out-of-plane displacements induced by applying ac voltage on the piezoelectric NW. Through the application of an electric field in various directions (axial and transverse) and by physical rotation of the NW with respect to the AFM cantilever (parallel or perpendicular), we measured all three piezoelectric constants in individual *c*-axis GaN NWs. Our results reveal that these NWs exhibit strong piezoelectricity in three dimensions up to six times that of the bulk value, which is particularly relevant to applications such as nanogenerators for energy harvesting. The method could be equally applied to other NW materials and crystal structures. Furthermore, we used the obtained constants in fully coupled finite element models to obtain voltage generation under flexural bending and tensile loading for *c*-, *a*-, and *m*-axis NWs.

GaN belongs to the hexagonal crystal group (6 mm), with six-fold symmetry and its piezoelectric tensor has three independent constants, d_{13}, d_{15}, and d_{33}.[31,32] The strain–electric field (ε_{ij}–E_k) relationship for piezoelectric material with 6 mm symmetry ($\varepsilon_{ij} = d_{ijk}E_k$) is expressed as

$$\begin{pmatrix} \varepsilon_{11} \\ \varepsilon_{22} \\ \varepsilon_{33} \\ 2\varepsilon_{23} \\ 2\varepsilon_{13} \\ 2\varepsilon_{12} \end{pmatrix} = \begin{pmatrix} 0 & 0 & d_{31} \\ 0 & 0 & d_{31} \\ 0 & 0 & d_{33} \\ 0 & d_{15} & 0 \\ d_{15} & 0 & 0 \\ 0 & 0 & 0 \end{pmatrix} \begin{pmatrix} E_1 \\ E_2 \\ E_3 \end{pmatrix} \tag{1}$$

The induced strain due to electric field in different directions is therefore expressed as $\varepsilon_{11} = \varepsilon_{22} = d_{31}E_3$, $\varepsilon_{33} = d_{33}E_3$, $2\varepsilon_{23} = d_{15}E_2$, $2\varepsilon_{13} = d_{15}E_1$, and $\varepsilon_{12} = 0$. For the *c*-axis GaN NWs (here studied), we define the coordinate system such that the three-axis is aligned with the long axis of the NW (*c*-axis [0001]), and one and two axes are in its cross-sectional plane, with the one axis being normal to the facet of the NW (Figure 1). In the converse piezoelectric effect, the voltage-induced displacement is measured to obtain the corresponding piezoelectric constant $d(pm/V)$. To obtain the three piezoelectric constants in the defined coordinate system, axial (E_3) and lateral (E_1 and E_2) electric fields must be applied on the NW. By applying a voltage in the axial direction, the piezoelectric constants d_{13} and d_{33} are obtained by measuring the corresponding displacements. The d_{15} constant is obtained by applying a transverse electric field (E_1) across the NW and measuring the strains ε_{23} or ε_{13}.[27,28] Figure 1 schematically shows the experimental setup for the measurement of the 3D piezoelectric matrix of an individual NW. In Figure 1b, the NW is shown on an insulating surface with its two ends clamped by electric contacts, which are used to apply an axial electric field. In Figure 1c, the NW is shown on a conductive substrate acting as an electric ground. An electric voltage is applied between a conductive AFM probe

dx.doi.org/10.1021/nl204043y | *Nano Lett.* 2012, 12, 970−976

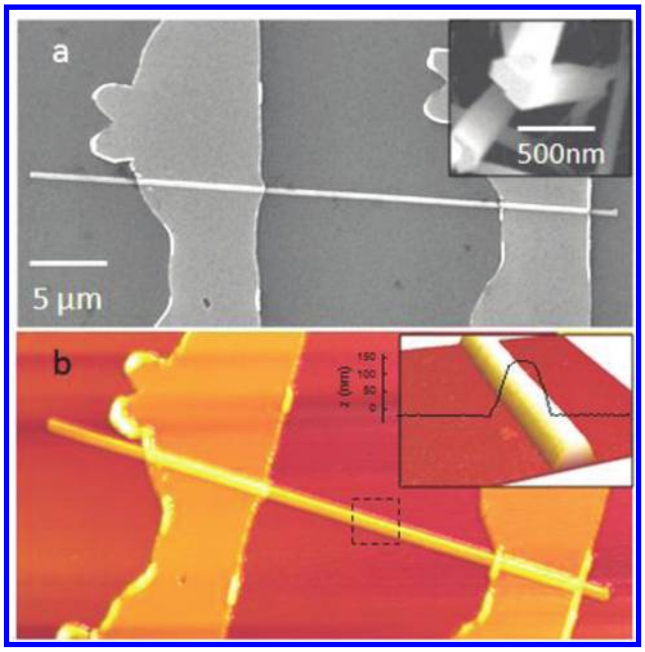

Figure 2. An individual GaN NW, H = 156 nm, with two electrodes Ti/Au (∼20/60 nm) deposited by thermal evaporation at its ends. (a) SEM image of the NW, inset showing cross sections of typical NWs with hexagonal geometry. (b) Corresponding tapping mode AFM topography image of the NW and electric contacts. Inset, high-magnification image of the area boxed with dashed lines showing the top surface of the NW, a half hexagon.

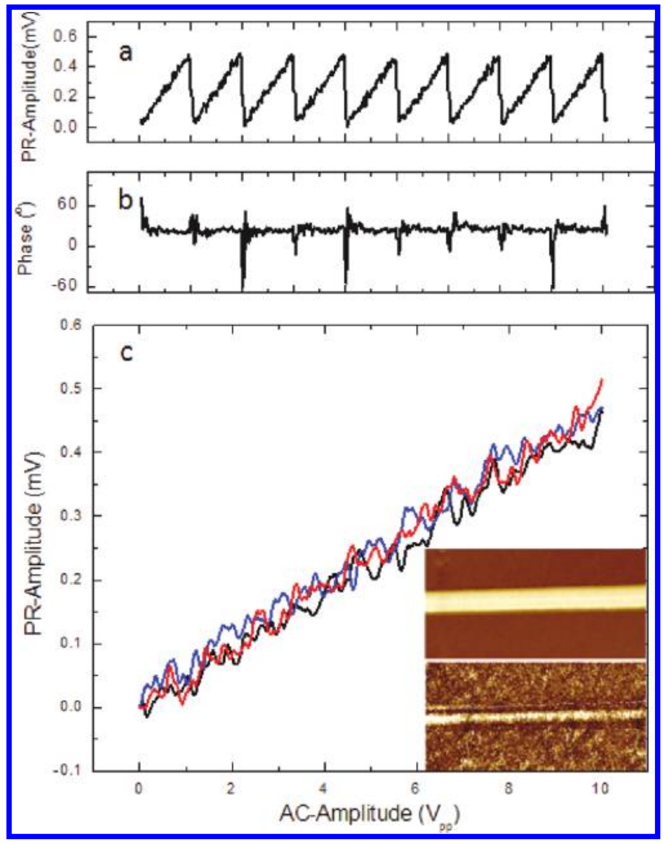

Figure 3. Measurement of piezoelectric-induced amplitude and phase on a single GaN NW. (a) Nine response curves obtained in the axial direction at a single point on a NW with H = 170 nm. The data clearly show the repeatability of the acquired responses. During each period, the input ac voltage of the function generator was swept in a ramp waveform from 0 to 10 V_{pp} in a 20 s period. (b) The corresponding phase response exhibits a constant phase, indicative of unipolar polarization in the NW. The jumps at the end of each period resulted from electrical noise in the function generator. (c) Piezoresponse amplitude acquired at three different points on the same NW, further showing repeatability of response along its axial direction. The linear amplitude response vs the input ac voltage is expected from linear electromechanical coupling. The inset shows a map of piezoresponse amplitude on a NW with H = 64 nm. AFM contact mode topography image (top), and simultaneously acquired lateral piezoresponse amplitude (bottom). The NW is distinctly resolved from the background noise on the Au-coated Si surface, with uniform piezoresponse along its length. The scan size is 2 μm.

and the grounded substrate to induce a transverse electric field in the NW. The displacement along the NW axis is measured in this case.

The GaN NWs used in this study were grown by molecular-beam epitaxy (MBE) in a catalyst-free process as previously reported.[33] The NWs are c-axis with the polar axis of the hexagonal wurtzite structure along the [0001] direction and the facets on$\{1\bar{1}00\}$ planes. Their single crystal structure was previously confirmed by transmission electron microscope (TEM) diffraction patterns. Nanowires were randomly dispersed using an isopropyl alcohol solution onto a Si wafer with a thermally grown SiO_2 insulating layer of thickness ∼400 nm. Metal contacts to the NWs were made using standard photolithography procedures followed by metal deposition and a lift-off process. Samples were first treated in a hexamethyldisilazane priming oven and spin coated by S1813 photoresist at 3000 rpm. They were then baked for 1 min at 110 °C on a hot plate and exposed to a deep UV light for 7 s followed by developing for 60 s in diluted 351 photoresist developer with the ratio of 1:3 with DI water. Patterns of ∼5 μm wide and ∼5 μm spacing were created in a Karl Suss MA6 optical mask aligner. The patterns were metalized by depositing Ti/Au (20/60 nm) in a thermal evaporator. Lift-off was performed in a warm acetone bath where samples were soaked for 15−30 min followed by rinsing with isopropyl alcohol and dried with a gentle flow of N_2 gas. For measurement of the shear piezoelectric constant, d_{15}, the NWs were randomly dispersed on a Si/SiO_2 surface coated with a thin layer (∼100 nm) of Au (bottom electrode).

Experiments were performed using an XE-120 Park AFM (Park Systems, CA) with a custom-designed piezoelectric measurement setup. Humidity was kept below ∼15% by enclosing the setup in a humidity chamber regulated by a flow of nitrogen (N_2) gas. An external lock-in amplifier (Stanford Research 830), a function generator (Stanford Research 5520), and a signal access module were used in the setup. Conductive Au/Cr-coated Si cantilevers (Mikromasch) with a nominal spring constant of k = 0.15 N/m were used for the measurements. The lateral sensitivity of the AFM cantilever was calibrated using optical-grade Y-cut single crystal $LiNbO_3$ with a well-defined piezoelectric constant.[15] The vertical sensitivity of the cantilever was calibrated by standard method of force−distance curve on a rigid substrate. For measurements, an ac voltage with a frequency of 10 kHz was applied. This frequency was identified from a frequency sweep to be away from the contact resonance of the cantilever and sample. The time constant of the lock-in amplifier was set to 100 and 3 ms for obtaining point measurement and piezoresponse maps, respectively.

Table 1. Experimentally Measured Piezoelectric Coefficients for Individual GaN NWs[a]

(a)	height (nm)	d_{33} (pm/V)	d_{13} (pm/V)	d_{15} (pm/V)
	156	12.4 ± 2.3	−10.1 ± 2.3 (−8.2 ± 1.3)	
	170	13.2 ± 0.4	−9.4 ± 0.9	
	64			−9.9 ± 0.7
	191			−10.5 ± 0.8

(b)	d_{33} (pm/V) [e_{33}] (C/N^2)	d_{13} (pm/V) [e_{13}] (C/N^2)	d_{15} (pm/V) [e_{15}] (C/N^2)	method [ref]
	12.8 [3.36]	−8.2 (−9.75) [−3]	−10.2 [−1.07]	SPM-based (NWs) current study
	[0.63]	[−0.32]	–	*ab initio* calculations[35]
	[0.73]	[−0.49]	–	*ab initio* calculations[36,37]
	2.7	−1.5	−1.8−3.3	density functional calculations[31]
	2	–		laser interferometer on thin films[38]
	–	–	−3.1	laser interferometer on thin films[39]

[a]Data in (a) are the mean values and standard deviation of the piezoelectric constant obtained for four different NWs investigated in this study and (b) are the computational and experimental data reported in the literature, for bulk and thin films, presented for comparison with the average values obtained in this study. (For d_{13} values obtained in two different configurations are reported, which are in agreement within 15%).

Prior to experiments, the NWs were inspected by SEM and AFM imaging (Figure 2) to ensure they were cleared of any photoresist residue after lift-off, which is essential for AFM measurements, and also to ensure their uniform geometry along their length. Through the AFM topography line profile, measurements were performed only on NWs resting on one of the facets and with another facet parallel to the plane of the cantilever, as shown in the AFM line profile given in the inset of Figure 2b. This ensured that the piezoelectric response was fully transferred to the AFM probe. For a NW sitting on one of the vertices, the response may not fully transfer to the measuring system. Furthermore, for quantitative measurement based on the setup shown in Figure 1, it is critical to place the *c*-axis of the NW (in this case, the long axis) perpendicular or parallel to the long axis of the AFM cantilever.[28] For a NW oriented at an angle of θ with respect to the long axis of the cantilever, only a fraction of the induced response, proportional to $\sin(\theta)$, would be transferred to the AFM cantilever. To achieve this orientation, the NWs were physically oriented with respect to the cantilever axis by rotating the holder while imaging with the optical system of the AFM followed by AFM scanning. For point measurements, the AFM tip was placed symmetrically in the middle of the top facet of the NW by scanning across the NW and setting the scan size to zero.

Figure 2 shows an individual GaN NW with two electrodes Ti/Au (~20 nm/60 nm) deposited by thermal evaporation at its two ends. Figure 2a is a scanning electron microscope (SEM) of the NW showing uniform geometry along its entire length. The inset shows the hexagonal cross-section, SEM image, of typical NWs. Figure 2b is the corresponding tapping mode AFM topography image. The height of the NW obtained from the topography image was H = 156 nm. The inset shows a high-magnification image of the area boxed within the dashed line. The overlaid line profile shows that the NW is sitting on one of the facets, with the other facet parallel to the surface, which is the preferred configuration for the experiment.

Figure 3 shows the measurements of the piezoresponse for a NW with H = 170 nm in the configuration shown in Figure 1a, where the ac voltage was applied between two electrodes and the torsional twist of the AFM cantilever measures the induced piezoresponse in the axial direction of the NW. Figure 3a shows nine consecutive piezoresponse curves obtained at a single point on the NW that clearly demonstrate the repeatability of the acquired responses. During each period, the input ac voltage of the function generator was swept in a ramp waveform from 0 to 10 V_{pp} in a 20 s period. Figure 3b depicts the corresponding phase response showing constant phase during voltage ramp and indication of unipolar polarization in the NW. The jumps at the end of each period resulted from the electrical noise in the function generator. Figure 3c shows the piezoresponses acquired at three different points on the same NW, which further shows repeatability of response along the axial direction. The linear amplitude response vs the input ac voltage is expected from piezoelectricity as the linear electromechanical coupling. The slope of the response curves at

Table 2. Summary of the Calculated Voltage Generation for GaN NWs with Different Crystallographic Orientations[a]

nanowire deformation	direction of the calculated voltage	generated voltage (V) with bulk properties	generated voltage (V) with NW properties	generated voltage (V) with NW properties where d_{33} = measured d_{13} = d_{15} = 0
c-axis bending	$[1\bar{1}00]$	0.1	0.3	0.3
c-axis tensile	[0001]	0.36	0.9	0.9
a-axis bending along [0001]	$[1\bar{2}10]$	1.09	2.2	0.006
m-axis bending along [0001]	middle cross-section basis along $[1\bar{2}10]$	0.52	1.7	0.55
a-axis - bending along $[1\bar{1}00]$	middle cross-section basis along $[1\bar{1}00]$	0.56	1.86	0.6
m-axis bending along $[1\bar{2}10]$	$[1\bar{1}00]$	1.10	2.18	0.006
a-axis tensile along $[1\bar{2}10]$	cross-section basis along $[1\bar{1}00]$	0.03	0.09	0.03
m-axis tensile along $[1\bar{1}00]$	cross section along [0001]	0.02	0.07	0.02

[a]Column one describes the type of the deformation along the mentioned axis, and column two represents the direction at which the generated voltage is reported. The two middle columns are the generated voltage for the cases when the bulk and the measured piezoelectric properties were used in the calculations. The column on the right is the special case when the shear piezoelectric properties were set to zero to highlight their contribution to the overall generated voltage.

each point (mV/V_{pp}) is used to obtain the piezoelectric constants of the NW by using the calibration of the lateral and vertical sensitivity (nm/mV) of the AFM probe.[15,27] The inset in the bottom right of Figure 3c shows the AFM contact mode topography image (top) and the map of piezoresponse amplitude on a NW with H = 64 nm, as it was reported in our previous study.[15] The response is obtained by applying a 10 V_{pp} between the AFM tip and the grounded substrate with a scanning speed of 0.25 Hz. The NW is distinctly resolved from the background noise on Au-coated Si surface, with uniform piezoresponse along its length, 2 μm. More than 100 response curves from 4 NWs in the range of H = 64−190 nm were analyzed. The results are summarized in Table 1a, for different diameters and piezoelectric constant. For each NW, the piezoresponse was acquired several times at the same point and was repeated at several different points along its length. Note that based on eq 1, $\varepsilon_{11} = \varepsilon_{22}$, hence the d_{13} constant could be measured by measuring either the lateral response (ε_{22}) or the vertical response (ε_{11}) on the NW under an axial electric field when the NW is placed parallel to the cantilever. There is a good agreement (within 15%) between the two measurements as presented in Table 1a. Reported in Table 1b are the piezoelectric constants of GaN obtained in other experimental and computational studies, for the bulk material, for comparison with the average values obtained in this study. Note the piezoelectric constants are commonly presented in units of pm/V (pC/N) or C/m^2 (which involves the elasticity parameters). For direct comparison with literate values, numbers in brackets from the current study are piezoelectric constants reported in units of C/m^2 after conversion using $e = dC$, where d is the piezoelectric matrix (pm/V), C is the elasticity matrix, and e is the piezoelectric coefficients relating polarization (P) and strain (ε), namely, $P = e\varepsilon$. For conversion, the bulk properties of GaN were used for the elasticity matrix.[6,34] Examination of the values reported in Table 1b reveals that the values identified in the current study for individual GaN NWs are 3−6 times larger than those previously reported for bulk GaN. It should also be noted that in PFM, the displacement is measured. Therefore, it is not expected that surface charges would play a role in the observed enhanced piezoelectricity. Particularly, the electrostatic effect ($\propto V^2$) would appear in the 2ω signal, where ω is the frequency of the applied electric field. By contrast, the linear piezoelectric effect measured in this study is based on the ω signal.

Similar strong piezoelectricity in 1D nanostructures was reported in the literature, such as for ZnO nanobelts[18] and peptide nanotubes.[29] A hypothesis for the measured size effect was advanced by Zhao et al.[18] They ascribed the effect to the defect-free nature of nanobelts. Our investigation based on quantum mechanical simulations revealed an increase in the polarization per unit volume as NW diameter decreases.[8] This increase is caused by NW lateral contraction, which becomes more prominent as NW diameter decreases. In the work here reported, we tested NWs in the range of 64−190 nm, which is outside the range of diameters investigated computationally. Clearly, further studies will be required, over a complete range of diameters from bulk to a few nanometers, to fully assess piezoelectric size effects.

As mentioned in the introductory paragraph, GaN NWs are proposed as energy harvesting elements in nanogenerators to convert mechanical deformation, such as tension and/or bending to electrical voltage. In order to assess the influence of this enhanced piezoelectricity in energy harvesting systems,

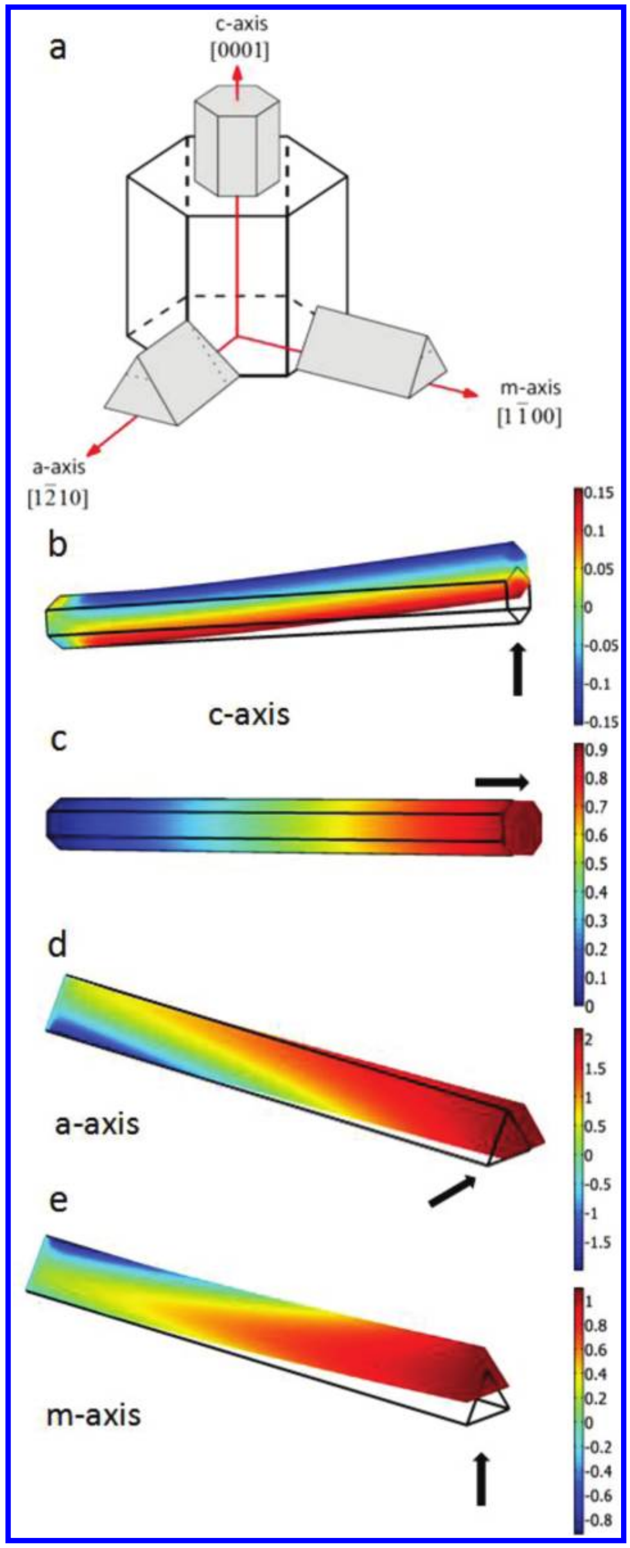

Figure 4. Piezo-potential distribution obtained from finite element modeling for GaN NWs with various crystallographic orientations. (a) The crystallographic orientation for hexagonal crystal, showing the growth axis for c-, a-, and m-axis GaN NWs. (b) and (c) are the flexural bending and tensile case for c-axis NWs, respectively. (d) and (e) are the flexural bending for a- and m-axis, respectively.

we performed finite element analysis for a fully coupled electromechanical system. The NW was assumed to be 100 nm in diameter with a length of 1 μm. The elastic properties employed in the simulations are bulk values.[34] The displacement boundary conditions were those of a cantilevered beam, with one end fixed and the other end loaded with a force of 80 nN, in bending or tension, to remain well within the elastic limit.[7] The electrical boundary condition was assumed to be grounded at the cantilevered end. We calculated voltage generation, under uniaxial tension and flexural bending for two different cases based on (i) bulk piezoelectric properties, $e_{33} = 0.73$ C/N^2, $e_{13} = e_{15} = -0.49$ C/N^2 [33] and (ii) the single NW properties identified in this study. The results are summarized in Table 2. The bending potential difference across the NW diameter is approximately 0.1 and 0.3 V, respectively. For the case of the tensile load, the potential varies linearly along the axial direction of the NW from 0 to 0.25 and 0.9 V, respectively. Figure 4b,c shows the piezo-potential map of the *c*-axis NWs under flexural bending and tension, respectively.

In addition, we performed finite element analysis for *a*-axis ($[1\bar{2}10]$) and *m*-axis ($[1\bar{1}00]$) NWs, with isosceles triangular cross section and basis length of 100 nm, under tension and bending. Figure 4d,e shows two representative deformations, and Table 2 provides more details about the voltage generation in the NWs. Similar to *c*-axis NWs, we compared the voltage generation for bulk vs single NW measured values. The data show an enhanced voltage generation of 2−3 times with respect to bulk. We also investigated the effect of the shear piezoelectric constants by setting it to zero. For *c*-axis NWs, the main contribution to the generated voltage in bending and tension originates from the d_{33} constant. Therefore, the calculations show no variation between the two cases as one would expect. However, for *a*- and *m*-axis NWs, calculations show that the shear piezoelectric constants contribute significantly to the generated voltage, as the value of the generated voltage drops to approximately zero by setting the shear piezoelectric constant to zero. These findings clearly highlight the importance of performing 3D piezoelectric measurements to fully identify all tensor components, which are needed to evaluate the voltage output in generators fabricated using piezoelectric NWs.

In summary, we have presented a method based on scanning force microscopy to obtain the 3D piezoelectric matrix of individual NWs. We applied the method to GaN NWs, and our results demonstrate that these NWs exhibit strong piezoelectricity in three-dimensions, with up to six times that of their bulk counterpart. Incorporating the obtained experimental values into finite element analysis, our results show that the NWs could have up to three times higher voltage generation respect to their bulk counterpart. These findings highlight applications of GaN NWs in nanogenerators for energy harvesting in self-powered nanodevices. The reported method is applicable to other NWs materials to obtain a full description of their piezoelectric properties.

■ AUTHOR INFORMATION

Corresponding Author

*Email: espinosa@northwestern.edu.

Present Address

[‡]Department of Physics, Saint Louis University, St. Louis, Missouri 63103, United States.

■ ACKNOWLEDGMENTS

We acknowledge Kris Bertness and Norman Sanford of the National Institute of Standards and Technology Optoelectronic Division for providing the NW samples. H.D.E. acknowledges the support of the NSF through awards DMR-0907196 and EEC-0647560 (NSF-NSEC). Use of the Center for Nanoscale Materials of the Argonne National Laboratory was supported by the U.S. Department of Energy, Office of Science, and Office of Basic Energy Sciences, under contract no. DE-ac02-06CH11357.

■ REFERENCES

(1) Yang, P.; Yan, R.; Fardy, M. *Nano Lett.* **2010**, *10*, 1529−1536.
(2) Wang, Z. L.; Song, J. *Science* **2006**, *312*, 242−246.
(3) Zhong, Z.; Qian, F.; Wang, D.; Lieber, C. M. *Nano Lett.* **2003**, *3*, 343−346.
(4) Johnson, J. C.; Choi, H.-J.; Knutsen, K. P.; Schaller, R. D.; Yang, P.; Saykally, R. J. *Nat. Mater.* **2002**, *1*, 106−110.
(5) Huang, Y.; Duan, X.; Cui, Y.; Lieber, C. M. *Nano Lett.* **2002**, *2*, 101−104.
(6) Bernal, R. A.; Agrawal, R.; Peng, B.; Bertness, K. A.; Sanford, N. A.; Davydov, A. V.; Espinosa, H. D. *Nano Lett.* **2011**, *11*, 548−555.
(7) Huang, C.-T.; Song, J.; Lee, W.-F.; Ding, Y.; Gao, Z.; Hao, Y.; Chen, L.-J.; Wang, Z. L. *J. Am. Chem. Soc.* **2010**, *132* (13), 4766−4771.
(8) Agrawal, R.; Espinosa, H. D. *Nano Lett.* **2011**.
(9) Agrawal, R.; Peng, B.; Gdoutos, E. E.; Espinosa, H. D. *Nano Lett.* **2008**, *8*, 3668−3674.
(10) Xu, S.; Qin, Y.; Xu, C.; Wei, Y.; UYang, R.; Wang, Z. *Nat. Nanotechnol.* **2010**, *5*, 366−373.
(11) Huang, C.-T.; Song, J.; Lee, W.-F.; Ding, Y.; Gao, Z.; Hao, Y.; Chen, L.-J.; Wang, Z. L. *J. Am. Chem. Soc.* **2010**, *132*, 4766−4771.
(12) Wang, X.; Song, J.; Zhang, F.; He, C.; Hu, Z.; Wang, Z. *Adv. Mater.* **2010**, *22*, 2155−2158.
(13) Xu, X.; Potie, A.; Songmuang, R.; Lee, J.; Bercu, B.; Baron, T.; Salem, B.; Montes, L. *Nanotechnology* **2011**, *22*, 105704.
(14) Lin, L.; Lai, C. H.; Hu, Y. F.; Zhang, Y.; Wang, X.; Xu, C.; Snyder, R. L.; Chen, L. J.; Wang, Z. L. *Nanotechnology* **2011**, *22*, 47.
(15) Minary-Jolandan, M.; Bernal, R. A.; Espinosa, H. D. *Mater. Res. Soc. Commun.*; available on Cambridge Journals Online; September 27, **2011**; doi:10.1557/mrc.2011.14 .
(16) Güthner, P.; Dransfeld, K. *Appl. Phys. Lett.* **1992**, *61*, 1137.
(17) Kolosov, O.; Gruverman, A.; Hatano, J.; Takahashi, K.; Tokumoto, H. *Phys. Rev. Lett.* **1995**, *74*, 4309−4312.
(18) Zhao, M.-H.; Wang, Z.-L.; Mao, S. X. *Nano Lett.* **2004**, *4*, 587−590.
(19) Wang, J.; Sandu, C. S.; Colla, E.; Wang, Y.; Ma, W.; Gysel, R.; Trodahl, H. J.; Setterb, N.; Kuball, M. *Appl. Phys. Lett.* **2007**, *90*, 133107.
(20) Yun, W. S.; Urban, J. J.; Gu, Q.; Park, H. *Nano Lett.* **2002**, *2*, 447−450.
(21) Wang, Z.; Hu, J.; Yu, M.-F. *Appl. Phys. Lett.* **2006**, *89*, 263119−3.
(22) Ke, T.-Y.; Chen, H.-A.; Sheu, H.-S.; Yeh, J.-W.; Lin, H.-N.; Lee, C.-Y.; Chiu, H.-T. *J. Phys. Chem. C* **2008**, *112*, 8827−8831.
(23) Wang, J.; Stampferı, C.; Roman, C.; Ma, W. H.; Setter, N.; Hierold, C. *Appl. Phys. Lett.* **2008**, *93*, 223101.
(24) Suyal, G.; Colla, E.; Gysel, R.; Cantoni, M.; Setter, N. *Nano Lett.* **2004**, *4*, 1339−1342.
(25) Feng, X.; Yang, B. D.; Liu, Y.; Wang, Y.; Dagdeviren, C.; Liu, Z.; Carlson, A.; Li, J.; Huang, Y.; Rogers, J. A. *ACS Nano* **2011**, *5*, 3326−3332.
(26) Qi, Y.; Kim, J.; Nguyen, T. D.; Lisko, B.; Purohit, P. K.; McAlpine, M. C. *Nano Lett.* **2011**, *1331−1336*, 1331−1336.
(27) Minary-Jolandan, M.; Yu, M.-F. *ACS Nano* **2009**, *3*, 1859−1863.
(28) Minary-Jolandan, M.; Yu, M.-F. *Nanotechnology* **2009**, *20*, 085706.
(29) Kholkin, A.; Amdursky, N.; Igor Bdikin, E. G.; Rosenman, G. *ACS Nano* **2010**, *4*, 610−614.
(30) Rodriguez, B. J.; Gruverman, A.; Kingon, A. I.; Nemanich, R. J. *J. Cryst. Growth* **2002**, *246*, 252−258.
(31) Bernardini, F.; Fiorentini, V. *Appl. Phys. Lett.* **2002**, *80*, 4145−4147.

(32) Newnham, R. E. *Properties of materials: anisotropy, symmetry,structure*. Oxford University Press: Oxford, U.K., 2005.
(33) Bertness, K. A.; Roshko, A.; Mansfield, L. M.; Harvey, T. E.; Sanford, N. A. *J. Cryst. Growth* **2008**, *310*, 3154−3158.
(34) Fonoberov, V. A.; Balandin, A. A. *J. Appl. Phys.* **2003**, *94*, 7178−7186.
(35) Shimada, K.; Sota, T.; Suzuki, K. *J. Appl. Phys.* **1998**, *84*, 4951−4958.
(36) Bernardini, F.; Fiorentini, V. *Phys. Rev. B* **1997**, *56*, R10024−R10027.
(37) Bernardini, F.; Fiorentini, V.; Vanderbilt, D. *Phys. Rev. Lett.* **1997**, *79*, 3958−3961.
(38) Muensit, S.; Guy, I. L. *Appl. Phys. Lett.* **1998**, *72*, 1896.
(39) Muensit, S.; Goldys, E. M.; Guy, I. L. *Appl. Phys. Lett.* **1999**, *75*, 3965−3967.